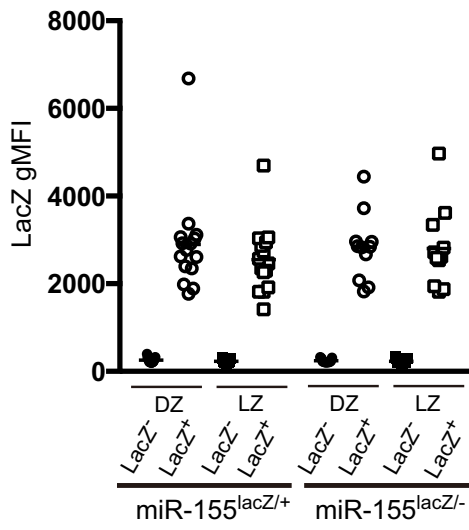


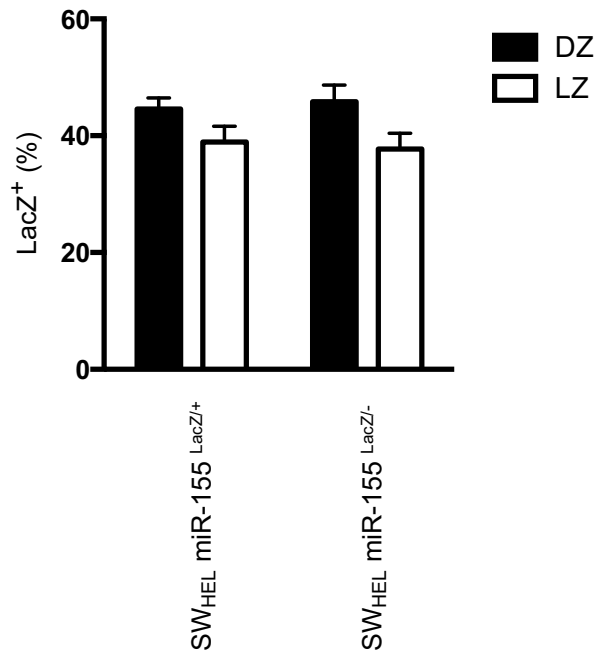
Supplementary 1 Lack of miR-155 does not affect LacZ activity or the proportion of LacZ<sup>+</sup> cells either in the DZ or in the LZ (related to Figure 2)

A

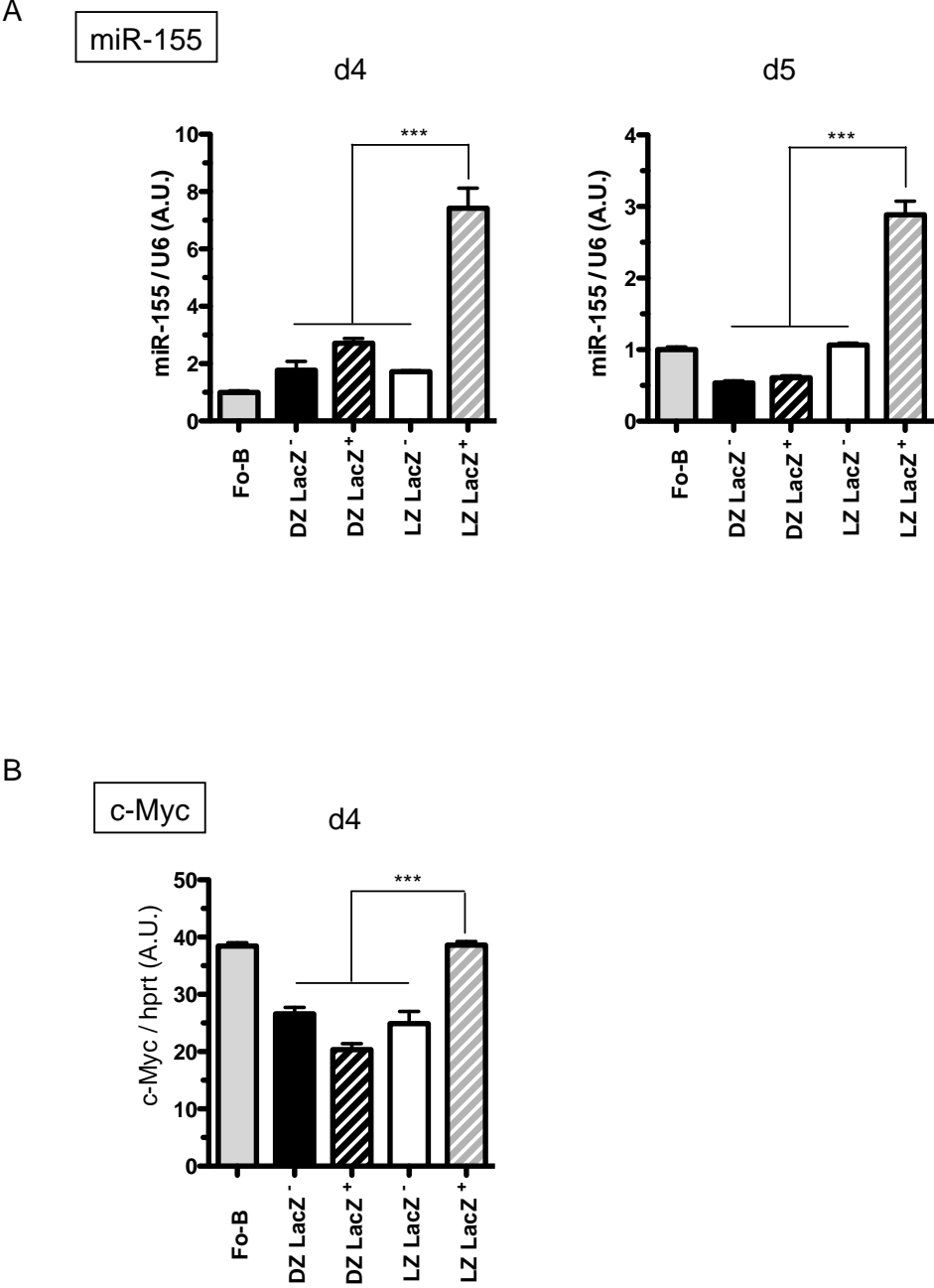


	SW <sub>HEL</sub> miR-155 <sup>LacZ/+</sup>	SW <sub>HEL</sub> miR-155 <sup>LacZ/-</sup>
DZ LacZ <sup>-</sup>	254.3 ± 14.55	241.4 ± 13.61
DZ LacZ <sup>+</sup>	2900 ± 296.9	2827 ± 231.0
LZ LacZ <sup>-</sup>	226.7 ± 12.45	230.8 ± 16.93
LZ LacZ <sup>+</sup>	2550 ± 199.3	2805 ± 275.9

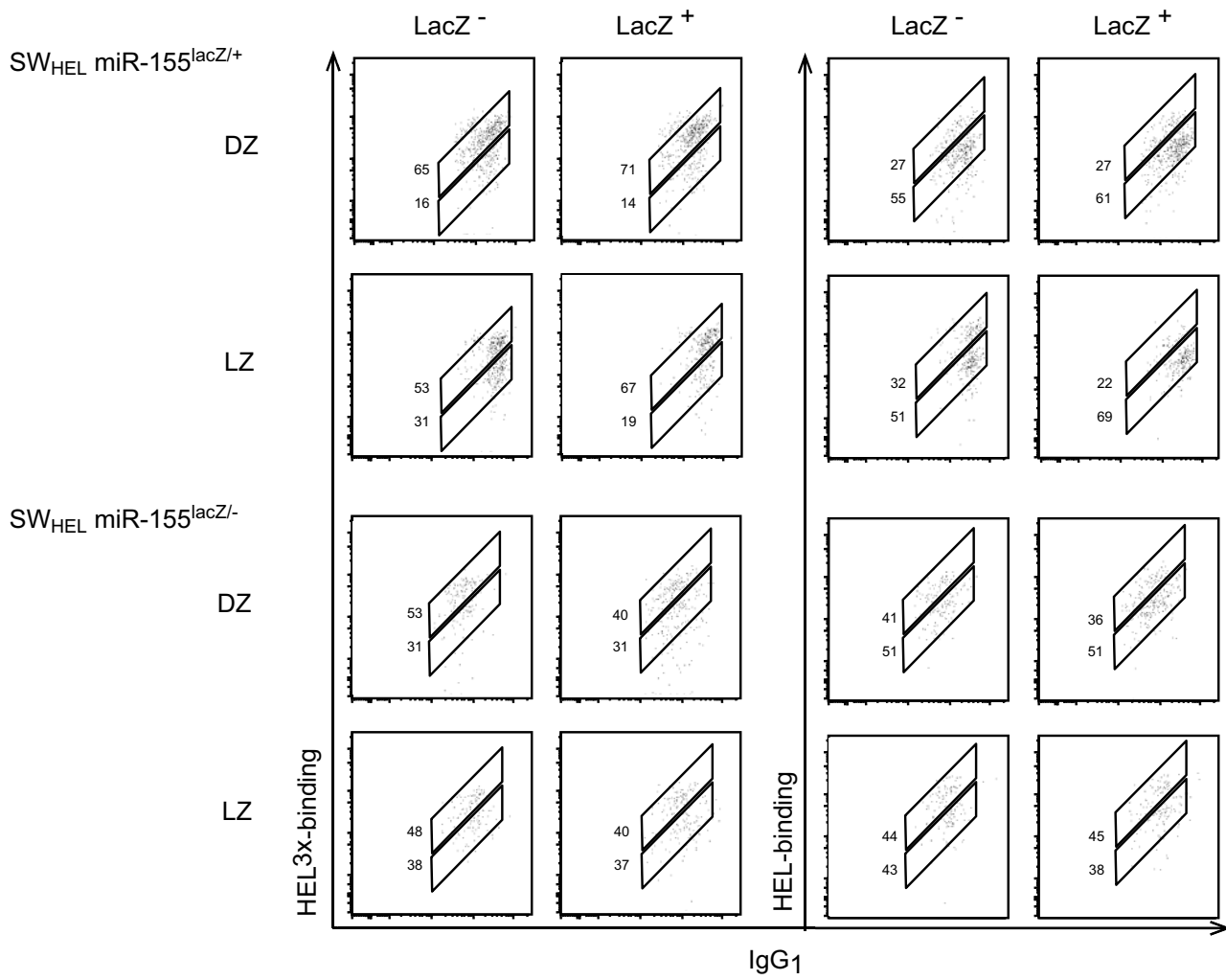
B



Supplementary 2 No substantial difference in expression of miR-155 and c-Myc between d4 and d5 (related to Figure 3)

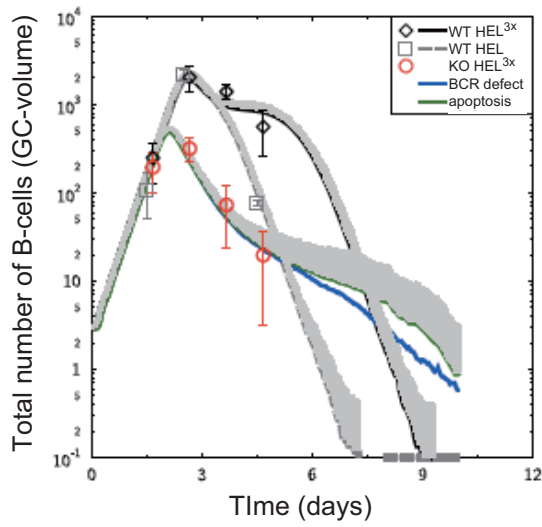


Supplementary 3 Affinity maturation assessment using FACS analysis of antigen binding  
(related to Figure 5)

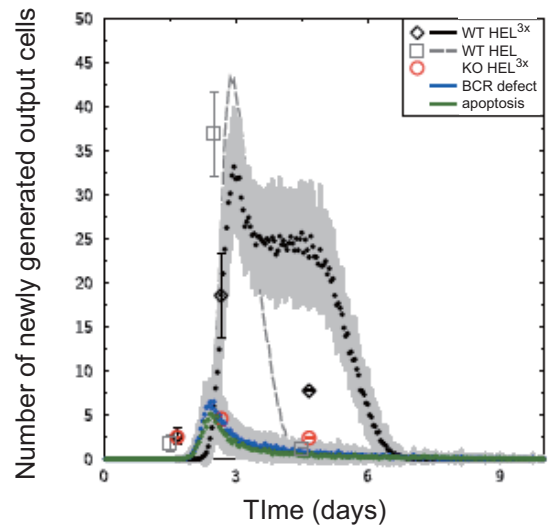


Supplementary 4 GC phenotype in miR-155 KO in silico (related to Figure 6)

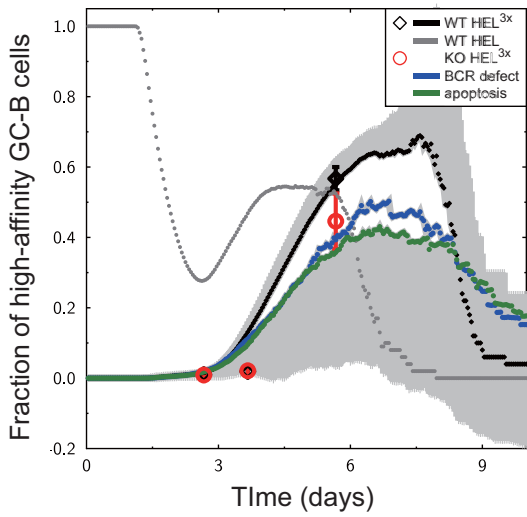
A



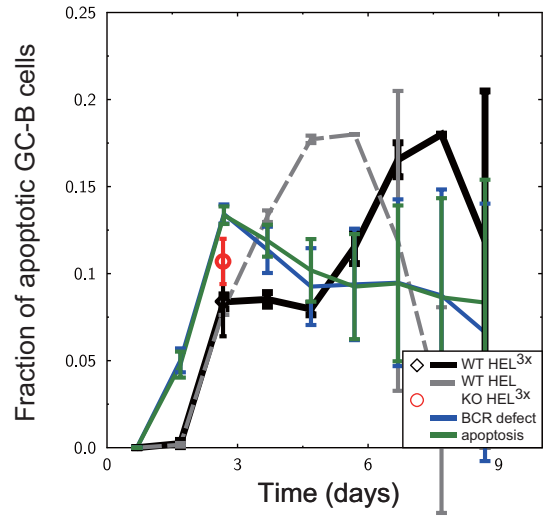
B



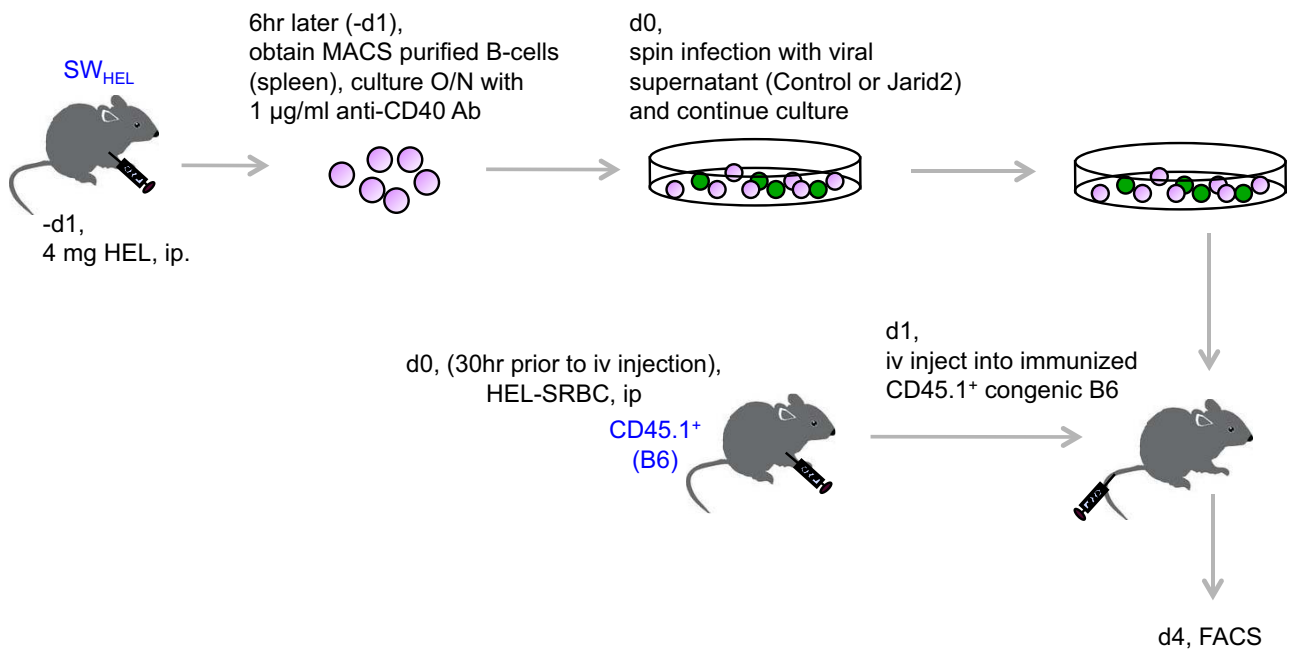
C



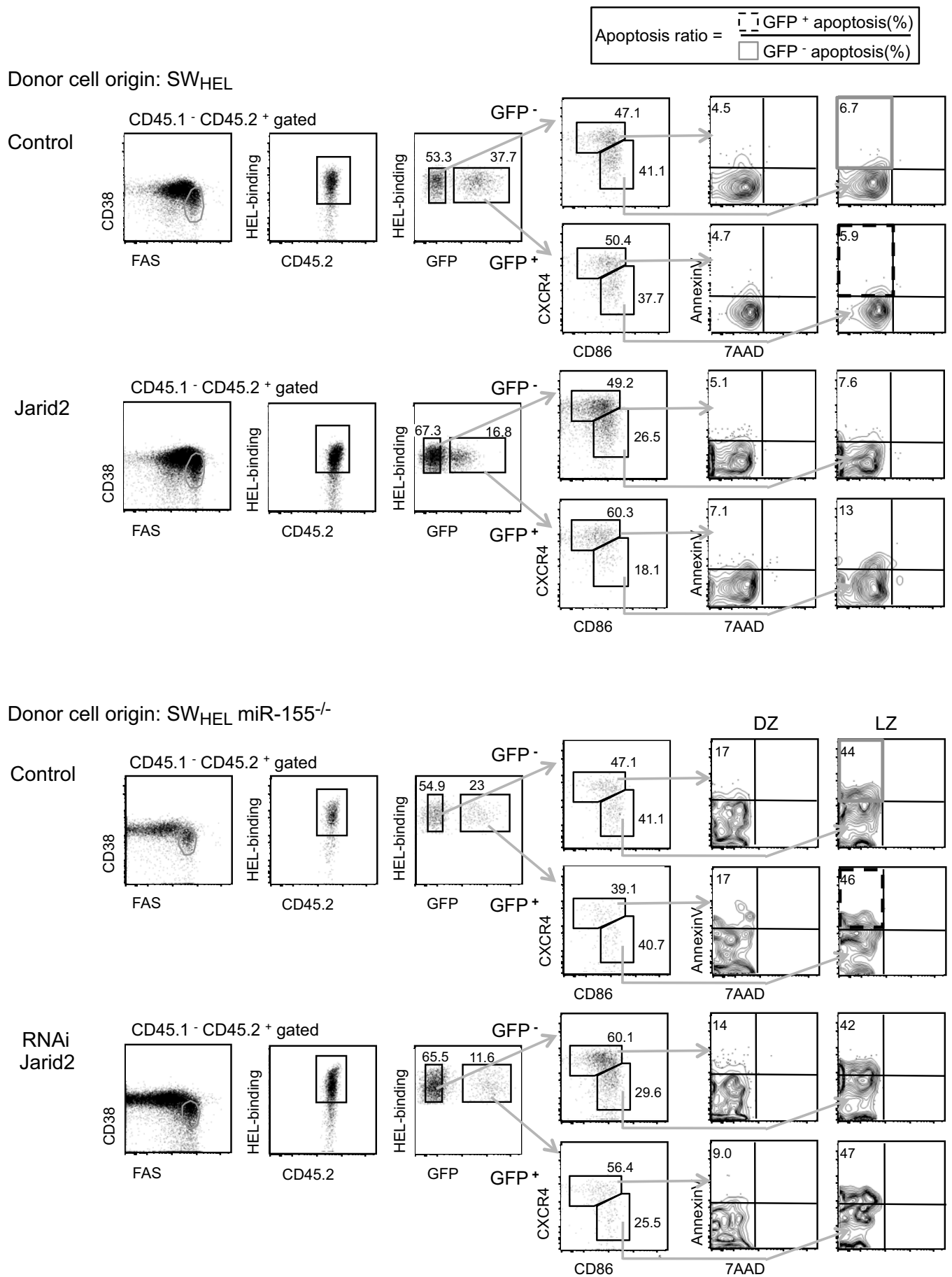
D



Supplementary 5 Methodology for the retroviral infection of ex-vivo isolated B-cells followed by adoptive transfer into congenic mice (related to Figure 7)



Supplementary 6 The miR-155 target gene Jarid2 regulates apoptosis of GC-B-cells  
(related to Figure 7)



## Supplementary figure legends:

### Supplementary Figure 1: Lack of miR-155 does not affect LacZ activity or the proportion of LacZ<sup>+</sup> cells either in the DZ or in the LZ (related Figure 2)

SW<sub>HEL</sub>-miR-155<sup>LacZ/+</sup> B-cells were adoptively transferred into CD45.1<sup>+</sup> congenic recipients which were injected with HEL<sup>3X</sup>-SRBC. Spleen cells from these mice were analyzed five days later. The graph shows geographic mean fluorescent intensity (gMFI) of LacZ (A) and the proportion of LacZ<sup>+</sup> cells of the indicated subsets (B). Each symbol represents a mouse on the left and the gMFI mean of the indicated fraction  $\pm$  SEM is shown on the right (A). Data correspond to the mean  $\pm$  SEM from the indicated number of independent sorting and flow cytometric experiments (B). SW<sub>HEL</sub>-miR-155<sup>LacZ/+</sup> n=15, SW<sub>HEL</sub>-miR-155<sup>LacZ/-</sup> n=11; n corresponds to the number of mice in the experiment.

### Supplementary Figure 2: No substantial difference in expression of miR-155 and c-Myc between d4 and d5 (related Figure 3)

SW<sub>HEL</sub>-miR-155<sup>LacZ/+</sup> B-cells were adoptively transferred into CD45.1<sup>+</sup> congenic recipients which were injected with HEL<sup>3X</sup>-SRBC. Spleen cells from these mice were sorted at the indicated day. miR-155 (A) and *c-Myc* transcripts (B) levels were analyzed by qRT-PCR and normalized by U6 or *Hprt*, respectively. Naïve-follicular B-cells (Fo-B) were sorted as B220<sup>+</sup> AA4.1<sup>-</sup> CD21/35<sup>int</sup> CD23<sup>hi</sup> cells from 2 naïve mice. The experiment shown is representative of two or three independent sorting experiments, d4 or d5, respectively. In each experiment, cDNA was prepared from sorted cells after pooling 5–10 mice. The mean  $\pm$  SEM is shown. \*\*\* p<0.001, one-way ANOVA followed by a Tukey's multiple comparisons post-test.

**Supplementary Figure 3: Affinity maturation assessment using FACS analysis of antigen binding (related to Figure 5)**

SW<sub>HEL</sub>-miR-155<sup>LacZ/+</sup> or SW<sub>HEL</sub>-miR155<sup>LacZ/-</sup> B-cells were adoptively transferred into CD45.1<sup>+</sup> recipients which were injected with HEL<sup>3X</sup>-SRBC. Spleen cells from these mice were analyzed four days later. Cells were gated as DZ or LZ followed by LacZ positivity. The FACS plot shows HEL-binding vs. IgG<sub>1</sub>. The top diagonal gate indicates cells of higher binding to HEL<sup>3X</sup> and HEL, right-hand and left-hand graphs, respectively, whereas the bottom gate corresponds to lower binding to BCRs to each antigen. Concatenated output of two files and three files for SW<sub>HEL</sub>-miR-155<sup>LacZ/+</sup> and SW<sub>HEL</sub>-miR155<sup>LacZ/-</sup>, respectively, are shown as a representative.

**Supplementary Figure 4: GC phenotype in miR-155 KO in silico (related to Figure 6)**

The WT simulations injected with HEL<sup>3X</sup> (simulations, black lines; in vivo experimental results, black open symbols and standard deviation) and with HEL (simulations, grey lines; in vivo experimental results, grey open symbols) and to the two best miR-155 KO in silico results are compared to the in vivo experimental result (red symbols). The in silico miR-155 KO was based on a defect of BCR signaling (blue lines) and on increased apoptosis of positively selected B-cells (green lines) (A-D). Mean and standard deviation (grey shades (A-C), bars (D)) of 50 simulations are shown. Only the upper error is shown because of the logarithmic scale (A).

**Supplementary Figure 5: Methodology for the retroviral infection of ex-vivo isolated B-cells followed by adoptive transfer into congenic mice (related to Figure 7)**

SW<sub>HEL</sub> mice were injected with HEL and 6 hrs later splenic B-cells were stimulated with anti-CD40 antibodies. The next day, cultured B-cells were retrovirally infected with either control or Jarid2 expressing vector and further cultured with anti-CD40 antibodies for one day. B-cells were then

adoptively transferred into CD45.1<sup>+</sup>-recipient mice which had been injected with HEL-SRBC 30 hrs earlier. Donor cells were analyzed on the indicated day by flow cytometry.

**Supplementary Figure 6: The miR-155 target gene Jarid2 regulates the apoptosis of GC-B-cells (related to Figure 7)**

The gating strategy. The graphs in Figure 7 show the proportion of AnnexinV<sup>+</sup> GFP<sup>+</sup> cells relative to AnnexinV<sup>+</sup> GFP<sup>-</sup> in the indicated conditions.

Supplementary Table1 Cell cycle status of each subset (related to Figure 5)

<b>SW<sub>HEL</sub>miR-155<sup>LacZ<sup>+</sup></sup></b>				
	DZ LacZ <sup>-</sup>	DZ LacZ <sup>+</sup>	LZ LacZ <sup>-</sup>	LZ LacZ <sup>+</sup>
G <sub>1</sub>	82.2 ± 1.66 <sup>###</sup>	48.7 ± 5.37	81.9 ± 1.32 <sup>*</sup>	60.4 ± 7.08
S	13.3 ± 0.938 <sup>###</sup>	40.2 ± 1.51	14.8 ± 1.10 <sup>*</sup>	30.9 ± 4.88
G <sub>2</sub> M	4.50 ± 1.47	11.1 ± 4.02	3.24 ± 0.740	8.71 ± 3.04

<b>SW<sub>HEL</sub>miR-155<sup>LacZ<sup>-</sup></sup></b>				
	DZ LacZ <sup>-</sup>	DZ LacZ <sup>+</sup>	LZ LacZ <sup>-</sup>	LZ LacZ <sup>+</sup>
G <sub>1</sub>	82.9 ± 1.54	51.9 ± 5.25	84.0 ± 0.790	60.6 ± 6.06
S	12.6 ± 1.54	38.1 ± 4.13	12.60 ± 0.763	27.3 ± 0.311
G <sub>2</sub> M	4.50 ± 1.24	9.96 ± 3.81	3.41 ± 0.726	8.19 ± 2.30

# DZ LacZ<sup>-</sup> vs. DZ LacZ<sup>+</sup>  
 \* LZ LacZ<sup>-</sup> vs. LZ LacZ<sup>+</sup>

Supplementary Table 2 Residual sum of squares for the different models of the effect of miR-155 knock out experiments (related to Figure 6)

<b>miR-155 KO effect</b>	<b>RSS value</b>	<b>Color in Figure 6</b>
Reduced cell cycle speed	3.5	Magenta
Reduced number of divisions during GC expansion	5.9	Light green
Reduced number of divisions during whole GC reaction	0.61	Orange
Defect of BCR leading to reduced antigen collection	0.50	Blue
Defect in antigen processing or presentation on peptide-MHC	2.9	Cyan
Increased apoptosis rate in the B-cell subset positively selected by T cells	0.51	Green

### **Supplementary Table1: Cell cycle status of each subset (related to Figure 5)**

Proportions of cells in G<sub>1</sub>, S and G<sub>2</sub>/M from the indicated DZ and LZ subsets derived from SW<sub>HEL</sub>-miR-155<sup>LacZ/+</sup> or SW<sub>HEL</sub>-miR-155<sup>LacZ/-</sup> B-cells. 1-1.3 × 10<sup>5</sup> cells of each subset were sorted, fixed and permeabilized with 4% paraformaldehyde followed by treatment with 0.1% PBS-Tween20. These cells were stained with DAPI. The mean of the indicated fraction ± SEM from five independent experiments is shown. Two-tailed paired t-test. #; Comparison between DZ LacZ<sup>-</sup> vs. DZ LacZ<sup>+</sup> and \*; LZ LacZ<sup>-</sup> vs. DZ LacZ<sup>-</sup>. The number of each symbol corresponds to the significance level: one, p<0.05 and three, p<0.0005. Two tailed unpaired t-test.

### **Supplementary Table2: Residual sum of squares for the different models of the effect of miR-155 knock out experiments (related to Figure 6)**

The Residual sum of squares (RSS) value was calculated based on the differences between simulation and in vivo experiment and normalized by the in vivo experimental value. Smaller RSS values depict a better agreement between the model and the in vivo data.